

Light-induced Odd-parity Magnetism in Conventional Collinear Antiferromagnets

Shengpu Huang,^{1,2} Zheng Qin,^{1,2} Fangyang Zhan,^{1,2} Dong-Hui Xu,^{1,2,*} Da-Shuai Ma,^{1,2,†} and Rui Wang^{1,2,‡}

¹*Institute for Structure and Function & Department of Physics & Chongqing Key Laboratory for Strongly Coupled Physics, Chongqing University, Chongqing 400044, People's Republic of China*

²*Center of Quantum materials and devices, Chongqing University, Chongqing 400044, People's Republic of China*
(Dated: August 6, 2025)

Recent studies have drawn growing attention on non-relativistic odd-parity magnetism in the wake of altermagnets. Nevertheless, odd-parity spin splitting is often believed to appear in non-collinear magnetic configurations. Here, using symmetry arguments and effective model analysis, we show that Floquet engineering offers a universal strategy for achieving odd-parity magnetism in two-dimensional (2D) collinear antiferromagnets under irradiation of periodic driving light fields such as circularly polarized light, elliptically polarized light, and bicircular light. A comprehensive classification of potential candidates for collinear monolayer or bilayer antiferromagnets is established. Strikingly, the light-induced odd-parity spin splitting can be flexibly controlled by adjusting the crystalline symmetry or the polarization state of incident light, enabling the reversal or conversion of spin-splitting. By combining first-principles calculations and Floquet theorem, we present illustrative examples of 2D collinear antiferromagnetic (AFM) materials to verify the light-induced odd-parity magnetism. Our work not only offers a powerful approach for uniquely achieving odd-parity spin-splitting with high tunability, but also expands the potential of Floquet engineering in designing unconventional compensated magnetism.

Introduction.— Recently, a novel category of collinear antiferromagnetic (AFM) phase dubbed altermagnetism, characterized by fully symmetry-compensated magnetic moments in real space and non-relativistic spin splitting in reciprocal space, has become the subject of intense recent studies [1–13]. The symmetry of altermagnets is dictated by spin space groups, which establish a new paradigm for understanding spin-dependent phenomena in crystalline materials [14–18]. Combining the advantages of ferromagnetism and antiferromagnetism in terms of spin splitting, altermagnets are predicted to exhibit a variety of fascinating properties, such as crystal Hall effects [19], spin-dependent conductivity [16, 20], large magnetoresistance effects [21, 22], as well as beyond [23–37]. To date, altermagnetism has been theoretically predicted and partially confirmed in a wide range of materials, stimulating broad interest in both fundamental studies and potential device applications [10, 38–40].

It is worth noting that altermagnetism, in its initial definition, features even-parity spin splitting with symmetries such as d -wave, g -wave, and i -wave [16, 20]. Following in the footsteps of counterpart altermagnets, non-relativistic odd-parity magnets have emerged as a prominent and rapidly evolving research frontier [41–46]. The odd-parity magnetism exhibits spin-splitting that is odd under a sign change of the momentum, analogous to the well-established Rashba and Dresselhaus spin-orbital coupling, suggesting its promising potential for spintronic devices [47–50]. Among various odd-parity magnets, p -wave magnetism is of particular interest as it corresponds to the long-sought unconventional p -wave superfluidity [51–53], and significant theoretical and experimental advances have been made in this field [41, 42, 44]. In particular, most recently, experimental evidence of p -wave spin splitting and its electrical control has been observed in NiI_2 [42]. Despite recent encouraging advancements,

odd-parity spin splitting reported to date has been limited to non-collinear magnetic configurations [41–43], which is in contrast to even-parity spin splitting observed in collinear altermagnets. Compared to collinear magnetic configurations, determining the ground state of non-collinear compensated magnets is considerably more complex, thus making their detailed studies by experiment difficult. As odd-parity magnetism represents one of the most intriguing features for spintronic applications, it is highly desirable to achieve this promising spin splitting in widely studied collinear antiferromagnets. Of equal importance is the realization of higher-order odd-parity spin splitting (such as f -wave or h -wave symmetry), which has remained largely unexplored.

We note that Floquet engineering with periodic driving has recently emerged as a powerful approach for tuning symmetry-related electronic properties [54–68], going beyond the well-established paradigm of static scenarios. Moreover, periodic light irradiation can impose magnetic symmetries from the magnetic space group [67]. Nevertheless, the prospect of dynamically controlling symmetry operators in the spin space group to achieve advanced manipulation of nonconventional magnetic properties, such as desirable spin splitting, is almost scarce. In this work, we demonstrate that Floquet engineering can provide a reliable strategy to achieving odd-parity spin splitting in two-dimensional (2D) conventional collinear antiferromagnets under light irradiation. Based on symmetry arguments and effective model analysis, we show how to achieve p -wave and f -wave spin splitting from collinear antiferromagnetism. All possible 2D candidates of f -wave spin-splitting are classified into three distinct lattice categories. Remarkably, this light-induced odd-parity spin splitting exhibits flexible tunability through precise control of the crystalline symmetry or the polarization state of incident light. As concrete demonstrations, through first-principles calculations combining with Floquet theory, we

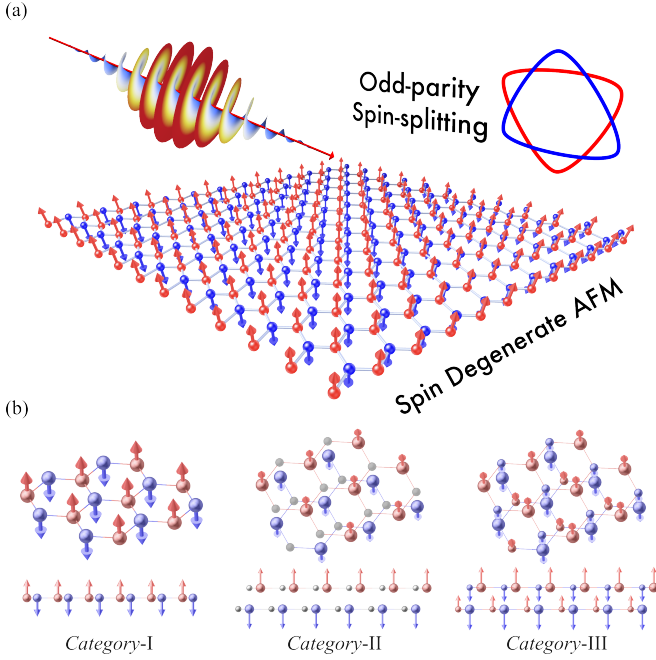


FIG. 1. Illustration of a general route to the odd-parity spin splitting in conventional antiferromagnets. (a) The conventional antiferromagnets comprises two sublattices that are connected by $[C_2 \parallel C_{2z}]$ or $[C_2 \parallel \mathcal{P}]$, schematically depicted by antiparallel red and blue spin arrows. The two sublattices form an inversion-symmetric pair, which gives rise to complete cancellation of spin splitting. The incident light propagates along the z -axis with its polarization plane parallel to the x - y plane. The two sublattices exhibit opposite optical responses, leading to the emergence of p -wave and f -wave spin splitting in the bands of the conventional antiferromagnets under circularly polarized light (CPL) irradiation. (b) The classification schematic of three material candidate categories of f -wave spin splitting: Hexagonal lattice with Néel-type magnetic configuration (Category-I), AFM bilayers composed of FM monolayers. (Category-II), AFM bilayers composed of Ferrimagnetic monolayers (Category-III). In all three categories, two sublattices with opposite magnetic moment must not be connected by $[C_2 \parallel \mathcal{O}', \mathcal{O}' \in \{\tau, \mathcal{M}_z\}]$.

verify the occurrence of f -wave spin splitting induced by circularly polarized light (CPL) in representative collinear antiferromagnets such as AFM MnPS_3 monolayer, FeCl_2 bilayer, and NiRuCl_6 bilayer, and reversing the chirality of CPL makes a sign change of this odd-parity spin splitting in the momentum space. More results of other possible candidates are given in the Supplementary Material (SM) [69]. Furthermore, we show that either symmetry breaking or irradiation with bicircular (BCL) or elliptically polarized light (EPL) can convert the light-induced spin polarization order from f -wave to p -wave.

Approach and symmetry analysis.— To clearly illustrate the construction of spin splitting with odd-parity polarization in a conventional collinear AFM system, we need to give a brief general description of the interaction between antiferromagnetism and periodic driving. The incident light is described by a time-periodic gauge field $\mathbf{A}(t) = \mathbf{A}(t + T)$, where $T = 2\pi/\omega$ denotes the optical period corresponding to

the light frequency ω . The eigenstates of the light-driven system are periodic $|\psi(t)\rangle = |\psi(t + T)\rangle = e^{-i\epsilon t} |\varphi(t)\rangle$, where $|\varphi(t)\rangle$ is dubbed Floquet states. In the framework of Floquet theory [57, 62–64], under the basis $|\varphi(t)\rangle = \sum_n e^{-in\omega} |u^n\rangle$, the time-dependent problem can be captured by Floquet Hamiltonian that is expressed in an infinite-dimensional extended Floquet space as

$$\sum_n (H_{m-n} - n\omega\delta_{m,n}) |\varphi_\alpha^n\rangle = \epsilon_\alpha |\varphi_\alpha^n\rangle, \quad (1)$$

where $H_{m-n}(\mathbf{k}) = \frac{1}{T} \int_0^T e^{i(m-n)\omega t} H(\mathbf{k}) dt$, and integer n is termed as the Floquet index. In the limit where the energy $\hbar\omega$ ($\hbar = 1$ is adopted in this work) of the driving light is large compared to the other energy scales, the periodically driven system can be described by effective Floquet Hamiltonian which reads

$$H_{\text{eff}}(\mathbf{k}) = H_0(\mathbf{k}) + \frac{[H_1(\mathbf{k}), H_{-1}(\mathbf{k})]}{\omega} + \mathcal{O}\left(\frac{1}{\omega^2}\right). \quad (2)$$

Firstly, we show that linearly polarized light irradiation does not induce spin splitting in conventional AFM materials (see the SM [69] for a detailed discussion). Then, we turn to the periodic driving light fields such as circularly polarized light (CPL), elliptically polarized light (EPL), and bicircular light (BCL). For CPL propagating along the z direction, the electromagnetic gauge field is given by $\mathbf{A}(t) = A_0(\eta \sin \omega t, \cos \omega t, 0)$, with $\eta = +1$ ($\eta = -1$) representing the circular polarization of the left-(right)-hand. For CPL irradiated systems with conventional AFM order, following the standard approach, one has

$$H_0(\mathbf{k}) = J_0(A_0|\delta|) [H_{\text{AFM}}(\mathbf{k}) - H(\mathbf{m}_\zeta)] + H(\mathbf{m}_\zeta). \quad (3)$$

Here, $H_{\text{AFM}}(\mathbf{k})$ is the Hamiltonian of conventional antiferromagnets, $H(\mathbf{m}_\zeta)$ represents the exchange interaction originating from the AFM order, $J_0(x)$ is the zeroth-order Bessel function of x . Note that, for simplicity, we consider only nearest-neighbor couplings and $|\delta|$ denotes the distance between adjacent sites. $H_0(\mathbf{k})$ corresponds to scaling the coupling strength in $H_{\text{AFM}}(\mathbf{k})$ by a constant factor $J_0(A_0|\delta|)$, implying the absence of spin splitting in $H_0(\mathbf{k})$, as shown in Fig. 2(a) for the AFM hexagonal lattice case. Thus, the potential light-induced spin splitting is completely determined by commutation $[H_1(\mathbf{k}), H_{-1}(\mathbf{k})] = \omega H'(\mathbf{k})$.

In 2D conventional antiferromagnets, the spin degeneracy is guaranteed by $[C_2 \parallel \mathcal{O}, \mathcal{O} \in \{\tau, \mathcal{P}, \mathcal{M}_z, C_{2z}\}]$, where C_2 is twofold rotation in spin space and \mathcal{O} is symmetry acting on lattice. In the SM [69], we show that for systems with symmetry $[C_2 \parallel \mathcal{O}', \mathcal{O}' \in \{\tau, \mathcal{M}_z\}]$, the spin degeneracy cannot be removed by light irradiation. Intriguingly, as schematically shown in Fig. 1, for system whose spin degeneracy is protected by $[C_2 \parallel \mathcal{P}]$ (or $[C_2 \parallel C_{2z}]$), the behavior is remarkably different. In this case, as discussed in detail below and schematically shown in Fig. 1 (a), the non-zero $H'(\mathbf{k})$ generates f -wave or p -wave spin splitting with odd-parity polarization. Furthermore, the irradiation of BCL and

EPL that reduce the spatial symmetry of CPL to C_{2z} convert the spin splitting from f -wave to p -wave.

Model.—Here, we first demonstrate the emergence of f -wave spin splitting in the Floquet bands of a conventional antiferromagnet modeled on a hexagonal lattice composed of spinful s orbitals. This occurs under the preservation of either the $[C_2 \parallel C_{6z}]$ or $[C_2 \parallel S_{6z}]$ symmetry, whose cubic operations correspond to $[C_2 \parallel C_{2z}]$ and $[C_2 \parallel P]$, respectively. The lattice is illustrated in Fig. 2 (a), and the tight-binding Hamiltonian of this AFM system reads

$$H = t \sum_{\langle i,j \rangle} c_i^\dagger c_j + \sum_i c_i^\dagger [\mu_\zeta \sigma_0 + \mathbf{m}_\zeta \cdot \boldsymbol{\sigma}] c_i + h.c., \quad (4)$$

where i (j) labels sites in sublattice A (B) whose index is $\zeta = 1$ ($\zeta = 2$), $c_i^\dagger = [c_{i,\uparrow}^\dagger, c_{i,\downarrow}^\dagger]$ ($c_i = [c_{i,\uparrow}, c_{i,\downarrow}]$) is the two component creation (annihilation) operator of electron at site i . The first term is the usual nearest-neighbor hopping term. The AFM exchange coupling and chemical potential are indicated by $\mathbf{m}_\zeta = m_\zeta (0, 0, 1)$ and μ_ζ , respectively. Guaranteed by $[C_2 \parallel C_{6z}]$ ($[C_2 \parallel S_{6z}]$) symmetry, one has $m_1 = -m_2$, and $\mu_1 = \mu_2 = 0$. Under the basis $[\varphi_\uparrow^A, \varphi_\uparrow^B, \varphi_\downarrow^A, \varphi_\downarrow^B]$, by performing the Fourier transformation, the explicit form of the Hamiltonian Eq. (4) can be written in momentum space as

$$H_{\text{AFM}}(\mathbf{k}) = \begin{bmatrix} 0 & \Delta(\mathbf{k}) \\ \Delta(\mathbf{k})^* & 0 \end{bmatrix} \tau_0 + (|m_\zeta| \sigma_z + |u_\zeta| \sigma_0) \tau_z \quad (5)$$

with $\Delta(\mathbf{k}) = t \sum_i e^{i\mathbf{k} \cdot \boldsymbol{\delta}_i}$, and $\boldsymbol{\delta}_i$ ($i = 1, 2, 3$) are the nearest-neighbor vectors, as inserted in Fig. 2 (a), $\boldsymbol{\tau}$ and $\boldsymbol{\sigma}$ are orbital and spin Pauli matrices, respectively.

By a straightforward derivation, $H_0(\mathbf{k})$ is given by $H_{\text{AFM}}(\mathbf{k}, t) \mapsto H_{\text{AFM}}(\mathbf{k}, tJ_0(\frac{aA_0}{\sqrt{3}}))$, with $a = 1$ is lattice constant. The spin-degenerate energy spectra of $H_{\text{AFM}}(\mathbf{k}, t)$ and $H_0(\mathbf{k})$ are given in Fig. 2 (b). The second term in Eq. (2) determines the potential spin splitting and is expressed as

$$\begin{aligned} \omega H'(\mathbf{k}) &= 8\sqrt{3}\eta J_1 \left(\frac{A_0}{\sqrt{3}} \right)^2 t^2 \prod_i \sin(k'_i/2) \sigma_0 \tau_z \\ &= f(\mathbf{k}) \sigma_0 \tau_z \end{aligned} \quad (6)$$

with $[k'_1, k'_2, k'_3] = [k_1, k_2, k_1 + k_2]$ and $k_{1,2}$ being reciprocal lattice vectors. Thus, the eigenvalues for the light-driven conventional antiferromagnet are obtained as

$$\epsilon_s(\mathbf{k}) = \pm \sqrt{\left| J_0 \left(\frac{A_0}{\sqrt{3}} \right) \Delta(\mathbf{k}) \right|^2 + (|m_\zeta| + sf(\mathbf{k})/\omega)^2}. \quad (7)$$

Here, the subscript $s = \pm 1$ represents the corresponding eigenstate of $\epsilon_s(\mathbf{k})$ is spin up and down, respectively. From Eq. (14), one finds that the CPL-driven conventional antiferromagnets and the eigenvalues of $H_{\text{eff}}(\mathbf{k})$, i.e., $E_s(\mathbf{k})$ exhibit four key features:

I: Due to $H'(k'_i = 0) \equiv 0$, the spin degeneracy is maintained along high-symmetry lines $k'_i = 0$.

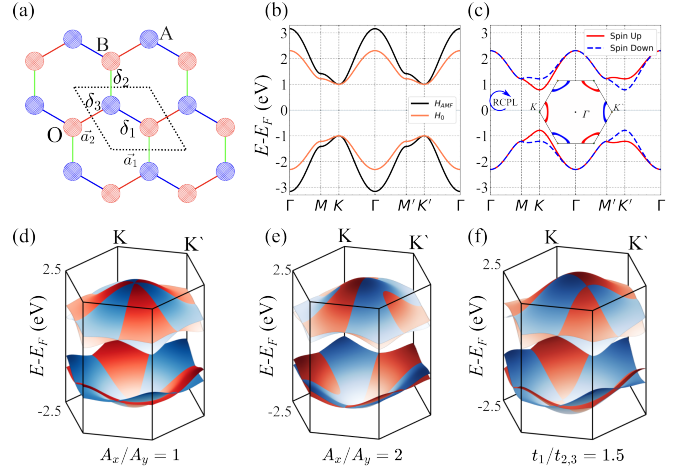


FIG. 2. A simple model for the light-induced odd-parity spin splitting and three categories of material candidates. (a) The illustration of the hexagonal lattice model with conventional AFM order. In the schematic representation, spin-up and spin-down magnetic atoms are depicted as red and blue spheres, respectively. (b) The spin-degenerate energy spectra of $H_{\text{AFM}}(\mathbf{k})$ and $H_0(\mathbf{k})$. (c) Spin-resolved energy spectra of conventional antiferromagnets under irradiation of right-handed CPL. The corresponding spin-resolved isoenergy surfaces at $E=1$ eV that exhibit f -wave spin splitting are presented as inset in (c), and the corresponding three-dimensional band structures are shown in (d). (e) Spin-resolved three-dimensional band structures with p -wave spin splitting in conventional antiferromagnets irradiated by EPL with amplitude ratio $A_x/A_y = 2$. (f) CPL induced p -wave spin splitting on AFM hexagonal lattice with biaxial strain, i.e., $t_1/t_{2,3} = 1.5$. In panels (c)-(f), the parameters $t = t_{2,3} = m_1 = -m_2 = 1$ eV and the light intensity of $eA_0/\hbar = 0.5 \text{ \AA}^{-1}$ are adopted.

II: The $E_s(\mathbf{k})$ is an odd function about s and \mathbf{k} , i.e., $E_s(\mathbf{k}) = E_{-s}(-\mathbf{k})$. And, $E_s(\mathbf{k})$ and $-E_{-s}(\mathbf{k})$ appear in pairs and $E_s(\mathbf{k}) \neq -E_{-s}(\mathbf{k})$ for arbitrary \mathbf{k} in 2D BZ. Thus, there is inevitable odd-parity spin splitting in CPL-driven conventional antiferromagnets, as shown in Fig. 2 (c).

III: From a symmetry perspective, the spin splitting within the BZ adheres to the symmetry of the system, i.e., $E_s(\mathbf{k}) = E_{-s}(\mathcal{O}^{-1}\mathbf{k})$ with \mathcal{O} is the spatial part of $[C_2 \parallel C_{6z}]^2$ or $[C_2 \parallel S_{6z}]^2$. Combining with features I~II, as inserted in Figs. 2 (c) and 2 (d), we obtain f -wave spin splitting.

IV: The appearance of τ_z in Eq. (6) implies that spin splitting originates from the opposite response of the two sublattices to circularly polarized light.

To bridge the gap between theoretical modeling and material prediction, we further incorporate next-nearest-neighbor couplings into Eq. (4). As presented in SM [69], features I~IV remain robust under this extension. Motivated by these features, we identify three distinct categories of candidate materials (designated *Category-I* through *Category-III*) for realizing f -wave spin splitting in conventional antiferromagnets, as schematically illustrated in Fig. 1 (b). *Category-I*: As detailed discussed, CPL enables f -wave spin splitting in a hexagonal monolayer with Néel-type magnetic

configuration. When such monolayers are stacked in a van der Waals magnetic multilayer, f -wave spin splitting can also be achieved by CPL (see SM [69] for details). *Category-II*: The light induced f -wave spin splitting can also be achieved in AFM bilayers composed of FM monolayers. It should be noted that feature IV dictates that the AFM bilayer necessarily violates symmetry $[C_2 \parallel \mathcal{O}', \mathcal{O}' \in \{\tau, \mathcal{M}_z\}]$. *Category-III*: One can also replace the monolayers employed in *Category-II* by ferrimagnetic (even fully compensated ferrimagnetic) monolayer. In SM [69], the light-induced f -wave spin splitting in lattices belong to *Category-II* and *Category-III* are discussed.

In addition to generating f -wave spin splitting, we show that the light-induced spin splitting can be effectively modulated through the polarization of incident light and the engineering of crystalline symmetries, thereby enabling the realization of p -wave spin splitting. As directly inferable from Eq. (4), turning the helicity of the incident circularly polarized light from right-handed ($\eta=1$) to left-handed ($\eta=-1$) leads to an reversal of the spin-splitting [69]. Furthermore, modifying the symmetry of incident light can give rise to p -wave spin splitting [69]. To this end, we employ BCL and EPL propagating along the z -direction. Their vector potentials are expressed respectively as $\mathbf{A}_{\text{EPL}}(t) = (A_x \sin \omega t, A_y \cos \omega t, 0)$ and $\mathbf{A}_{\text{BCL}}(t) = \sqrt{2} A_0 \text{Re} [e^{-i\omega_1 t}, e^{-i\kappa\omega_1 t}, 0]$ with κ denoting the frequency ratio between the right- and left-handed components constituting the BCL. In this case, although analytically deriving the explicit form of $H'(\mathbf{k})$ and corresponding eigenvalues is highly cumbersome, the numerical results can be readily obtained via Eq. (2). Fig. 2(e) shows that, in the presence of elliptical polarized light (EPL) with an amplitude ratio of $A_x/A_y = 2$, the energy spectrum of conventional antiferromagnets exhibits p -wave spin splitting.

We now investigate the p -wave spin splitting induced by CPL in conventional collinear antiferromagnets. To achieve distinct spin polarization orders, we begin by reducing the spatial symmetries of the lattice model described in Eq. (4). Applying uniaxial strain along the $[100]$ and $[110]$ directions lowers the point group symmetry of the hexagonal lattice shown in Fig. 2(a) from D_6 to C_2 and D_2 , respectively. As illustrated in Fig. 2(f), taking the strain along $[110]$ as an example, the energy bands exhibit p -wave spin polarization order under CPL irradiation.

Material realization of odd-parity spin splitting.— With the theoretical framework in place, we now shift focus from theoretical design concepts to the material realization of the light-induced odd-parity spin splitting in conventional antiferromagnets. According to the theoretical analysis established above, the AFM system must satisfy two constraints: (i) preservation of either $[C_2 \parallel C_{2z}]$ or $[C_2 \parallel \mathcal{P}]$ symmetry and (ii) composed of two sublattices that cannot be connected by $[C_2 \parallel \mathcal{O}', \mathcal{O}' \in \{\tau, \mathcal{M}_z\}]$. Based on theoretical analysis and density functional theory calculations, we predict three candidate materials (see Figs. 3(a)–3(c)) for realizing f -wave spin splitting: monolayer MnPS_3 , bilayer FeCl_2 , and bilayer NiRuCl_6 , corresponding to *Category-I*, *-II*, and

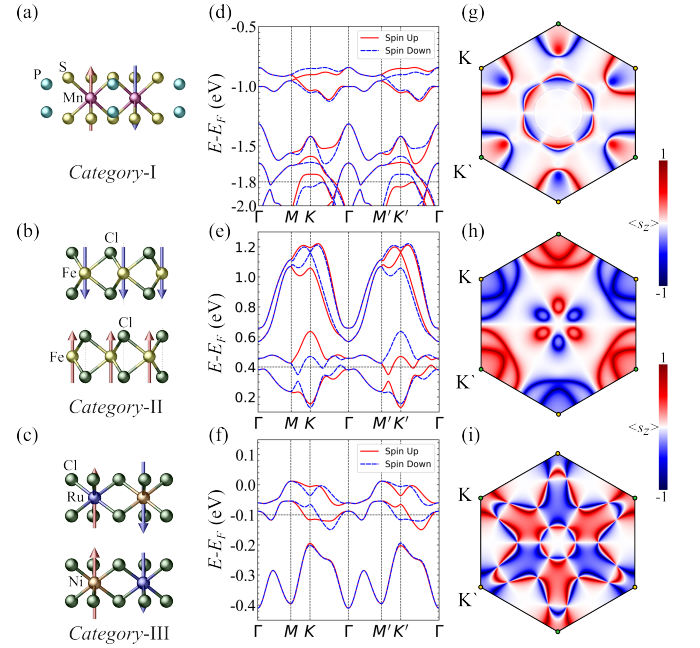


FIG. 3. CPL induced f -wave spin splitting in representative materials, i.e., AFM MnPS_3 monolayer (*Category-I*), AFM FeCl_2 bilayer (*Category-II*), and AFM NiRuCl_6 bilayer (*Category-III*). (a)–(c) The side-view and bird-view of crystal structure and magnetic order of AFM MnPS_3 monolayer, AFM FeCl_2 bilayer, and AFM NiRuCl_6 bilayer. (d)–(f) The spin-resolved band structures (curves in red solid represent the spin-up state) along high-symmetry lines of the AFM MnPS_3 monolayer, AFM FeCl_2 bilayer, and AFM NiRuCl_6 bilayer under irradiation of CPL with a light intensity of $eA_0/\hbar = 0.3 \text{ \AA}^{-1}$ and the photon energy of this light $\hbar\omega = 10 \text{ eV}$. The light irradiation preserves the spin degeneracy along the high-symmetry line Γ -M while lifting the degeneracy at other arbitrary \mathbf{k} -point. (g)–(i) The spin-resolved isoenergy surfaces with f -wave spin splitting of the AFM MnPS_3 monolayer at -1.8 eV , the AFM FeCl_2 bilayer at 0.4 eV , and the AFM NiRuCl_6 bilayer at -0.1 eV .

–III, respectively. Notably, all three candidate materials have been extensively studied, with experimentally confirmed ground-state magnetic structures consistent with the required symmetry constraints.

Through first-principles calculations (see the SM [69] for calculation details), we first confirm the intrinsic spin-degenerate band structure in the three types of candidates. Then we apply a counterclockwise CPL to MnPS_3 , FeCl_2 and NiRuCl_6 . The photon energy of this light is set as $\hbar\omega=10 \text{ eV}$ to meet the high-frequency approximation condition. Figures. 3(d)–3(f) presents the calculated spin-resolved band structures of MnPS_3 , FeCl_2 and NiRuCl_6 under the light intensity of $eA_0/\hbar = 0.3 \text{ \AA}^{-1}$. Figs. 3(d)–3(f) show that light irradiation lifts the spin degeneracy at generic \mathbf{k} -points while preserving it along the high-symmetry Γ -M line. The spin-resolved isoenergy surfaces for MnPS_3 at -1.8 eV , FeCl_2 at 0.4 eV and NiRuCl_6 at -0.1 eV are presented in Figs. 3(g)–3(i), confirming the appearance of light-induced f -wave spin splitting in these three classes of conventional antiferromagnets.

Before concluding, using the AFM FeCl₂ bilayer as an example, we demonstrate the tunability of f -wave spin polarization order via precise control of the light polarization and crystalline symmetry (see SM [69] for details). We apply counterclockwise BCL, EPL, uniaxial strain along the [110] or [100] direction to manipulate the light-induced f -wave spin polarization order in AFM FeCl₂ bilayer system. Owing to the breaking of the $[C_2 \parallel S_{6z}]$, the application of BCL, EPL, or strain combined with CPL leads to p -wave spin splitting, as shown in Fig.S7 and Fig.S8 [69]. These observations are fully consistent with the theoretical analysis presented in previous sections.

Conclusions.—Summarily, we present a universal approach for achieving and controlling odd-parity spin splitting in conventional collinear AFM systems through irradiation of light. Employing low-energy effective models alongside symmetry analysis, we point out the symmetry requirements for achieving f - and p -wave spin splitting. Materials exhibiting f -wave spin splitting can be classified into three distinct lattice categories. Using first-principles calculations, we identify the extensively studied AFM MnPS₃ monolayer, AFM FeCl₂ bilayer, and AFM NiRuCl₆ bilayer as promising candidates for the realization of f -wave spin splitting via CPL irradiation. Notably, beyond the materials discussed in the main text, compounds such as MnBi₂Te₄, RuO₂ (1H phase) and MnX₂ ($X = S, Se, Te$) (see Table SI of the SM [69] for additional candidates) also provide promising platforms for realizing of odd-parity spin splitting. Furthermore, the odd-parity spin splitting is verified to be flexibly controlled by manipulating the polarization of the incident light and crystalline symmetry, enabling reversal or conversion of spin-splitting. In light of the recent experimental realization of non-collinear p -wave magnets, our proposed approach for achieving and manipulating collinear p -wave and f -wave magnets paves the way for discovering promising candidates for next-generation spintronic devices, including high-density magnetic memories and terahertz nano-oscillators.

Note added.—Recently, we became aware of an independent work by Bo Li *et.al.* [arXiv.2507.22884] addressing the Floquet driven non-relativistic spin-splitting [70].

Acknowledgments.—This work was supported by the National Natural Science Foundation of China (NSFC, Grants No. 12222402, No. 92365101, No. 12347101, and No. 12204074), the Natural Science Foundation of Chongqing (Grants No. 2023NSCQ-JQX0024 and No. CSTB2022NSCQMSX0568).

* donghuixu@cqu.edu.cn

† mads@cqu.edu.cn

‡ rcwang@cqu.edu.cn

- [1] S. Hayami, Y. Yanagi, and H. Kusunose, Bottom-up design of spin-split and reshaped electronic band structures in antiferromagnets without spin-orbit coupling: Procedure on the basis of augmented multipoles, *Phys. Rev. B* **102**, 144441

(2020).

- [2] H. Bai, L. Han, X. Y. Feng, Y. J. Zhou, R. X. Su, Q. Wang, L. Y. Liao, W. X. Zhu, X. Z. Chen, F. Pan, X. L. Fan, and C. Song, Observation of spin splitting torque in a collinear antiferromagnet RuO₂, *Phys. Rev. Lett.* **128**, 197202 (2022).
- [3] I. Mazin (The PRX Editors), Editorial: Altermagnetism—a new punch line of fundamental magnetism, *Phys. Rev. X* **12**, 040002 (2022).
- [4] C. Wu, K. Sun, E. Fradkin, and S.-C. Zhang, Fermi liquid instabilities in the spin channel, *Phys. Rev. B* **75**, 115103 (2007).
- [5] R. D. Gonzalez Betancourt, J. Zubáć, R. Gonzalez-Hernandez, K. Geishendorf, Z. Šobáň, G. Springholz, K. Olejník, L. Šmejkal, J. Sinova, T. Jungwirth, S. T. B. Goennenwein, A. Thomas, H. Reichlová, J. Železný, and D. Kriegner, Spontaneous anomalous hall effect arising from an unconventional compensated magnetic phase in a semiconductor, *Phys. Rev. Lett.* **130**, 036702 (2023).
- [6] S. Hayami, Y. Yanagi, and H. Kusunose, Momentum-dependent spin splitting by collinear antiferromagnetic ordering, *J. Phys. Soc. Jpn* **88**, 123702 (2019).
- [7] P. A. McClarty and J. G. Rau, Landau theory of altermagnetism, *Phys. Rev. Lett.* **132**, 176702 (2024).
- [8] J. Krempaský, L. Šmejkal, S. D'souza, M. Hajlaoui, G. Springholz, K. Uhlířová, F. Alarab, P. Constantinou, V. Strocov, D. Usanov, *et al.*, Altermagnetic lifting of kramers spin degeneracy, *Nature* **626**, 517 (2024).
- [9] L. Bai, W. Feng, S. Liu, L. Šmejkal, Y. Mokrousov, and Y. Yao, Altermagnetism: Exploring new frontiers in magnetism and spintronics, *Adv. Funct. Mater* **34**, 2409327 (2024).
- [10] C. Song, H. Bai, Z. Zhou, L. Han, H. Reichlová, J. H. Dil, J. Liu, X. Chen, and F. Pan, Altermagnets as a new class of functional materials, *Nat. Rev. Mater.*, 1 (2025).
- [11] S.-W. Cheong and F.-T. Huang, Altermagnetism classification, *npj Quantum Mater.* **10**, 38 (2025).
- [12] F. Zhang, X. Cheng, Z. Yin, C. Liu, L. Deng, Y. Qiao, Z. Shi, S. Zhang, J. Lin, Z. Liu, *et al.*, Crystal-symmetry-paired spin–valley locking in a layered room-temperature metallic altermagnet candidate, *Nat. Phys.*, 1 (2025).
- [13] M. Hu, X. Cheng, Z. Huang, and J. Liu, Catalog of c -paired spin-momentum locking in antiferromagnetic systems, *Phys. Rev. X* **15**, 021083 (2025).
- [14] W. Brinkman and R. J. Elliott, Theory of spin-space groups, *Proc. R. Soc. A* **294**, 343 (1966).
- [15] P. Liu, J. Li, J. Han, X. Wan, and Q. Liu, Spin-group symmetry in magnetic materials with negligible spin-orbit coupling, *Phys. Rev. X* **12**, 021016 (2022).
- [16] L. Šmejkal, J. Sinova, and T. Jungwirth, Emerging research landscape of altermagnetism, *Phys. Rev. X* **12**, 040501 (2022).
- [17] Z. Xiao, J. Zhao, Y. Li, R. Shindou, and Z.-D. Song, Spin space groups: Full classification and applications, *Phys. Rev. X* **14**, 031037 (2024).
- [18] Y. Jiang, Z. Song, T. Zhu, Z. Fang, H. Weng, Z.-X. Liu, J. Yang, and C. Fang, Enumeration of spin-space groups: Toward a complete description of symmetries of magnetic orders, *Phys. Rev. X* **14**, 031039 (2024).
- [19] L. Šmejkal, R. González-Hernández, T. Jungwirth, and J. Sinova, Crystal time-reversal symmetry breaking and spontaneous hall effect in collinear antiferromagnets, *Sci. Adv.* **6**, eaaz8809 (2020).
- [20] L. Šmejkal, J. Sinova, and T. Jungwirth, Beyond conventional ferromagnetism and antiferromagnetism: A phase with nonrelativistic spin and crystal rotation symmetry, *Phys. Rev. X* **12**, 031042 (2022).
- [21] L. Šmejkal, A. B. Hellenes, R. González-Hernández, J. Sinova,

- and T. Jungwirth, Giant and tunneling magnetoresistance in unconventional collinear antiferromagnets with nonrelativistic spin-momentum coupling, *Phys. Rev. X* **12**, 011028 (2022).
- [22] D.-F. Shao, S.-H. Zhang, M. Li, C.-B. Eom, and E. Y. Tsymlal, Spin-neutral currents for spintronics, *Nat. Commun.* **12**, 7061 (2021).
- [23] X. Zhou, W. Feng, X. Yang, G.-Y. Guo, and Y. Yao, Crystal chirality magneto-optical effects in collinear antiferromagnets, *Phys. Rev. B* **104**, 024401 (2021).
- [24] H.-Y. Ma, M. Hu, N. Li, J. Liu, W. Yao, J.-F. Jia, and J. Liu, Multifunctional antiferromagnetic materials with giant piezomagnetism and noncollinear spin current, *Nat. Commun.* **12**, 2846 (2021).
- [25] T. Aoyama and K. Ohgushi, Piezomagnetic properties in altermagnetic mnte, *Phys. Rev. Mater.* **8**, L041402 (2024).
- [26] H. Reichlova, R. Lopes Seeger, R. González-Hernández, I. Kounta, R. Schlitz, D. Krieger, P. Ritzinger, M. Lammel, M. Leiviskä, A. Birk Hellenes, *et al.*, Observation of a spontaneous anomalous hall response in the Mn_3Si_3 d-wave altermagnet candidate, *Nat. Commun.* **15**, 4961 (2024).
- [27] R. He, D. Wang, N. Luo, J. Zeng, K.-Q. Chen, and L.-M. Tang, Nonrelativistic spin-momentum coupling in antiferromagnetic twisted bilayers, *Phys. Rev. Lett.* **130**, 046401 (2023).
- [28] B. Pan, P. Zhou, P. Lyu, H. Xiao, X. Yang, and L. Sun, General stacking theory for altermagnetism in bilayer systems, *Phys. Rev. Lett.* **133**, 166701 (2024).
- [29] Y. Liu, J. Yu, and C.-C. Liu, Twisted magnetic van der waals bilayers: An ideal platform for altermagnetism, *Phys. Rev. Lett.* **133**, 206702 (2024).
- [30] S. Zeng and Y.-J. Zhao, Bilayer stacking a -type altermagnet: A general approach to generating two-dimensional altermagnetism, *Phys. Rev. B* **110**, 174410 (2024).
- [31] X. Zhu, X. Huo, S. Feng, S.-B. Zhang, S. A. Yang, and H. Guo, Design of altermagnetic models from spin clusters, *Phys. Rev. Lett.* **134**, 166701 (2025).
- [32] C. W. J. Beenakker and T. Vakhtel, Phase-shifted andreev levels in an altermagnet josephson junction, *Phys. Rev. B* **108**, 075425 (2023).
- [33] J. A. Ouassou, A. Brataas, and J. Linder, dc josephson effect in altermagnets, *Phys. Rev. Lett.* **131**, 076003 (2023).
- [34] D. Zhu, Z.-Y. Zhuang, Z. Wu, and Z. Yan, Topological superconductivity in two-dimensional altermagnetic metals, *Phys. Rev. B* **108**, 184505 (2023).
- [35] M. Gu, Y. Liu, H. Zhu, K. Yananose, X. Chen, Y. Hu, A. Stroppa, and Q. Liu, Ferroelectric switchable altermagnetism, *Phys. Rev. Lett.* **134**, 106802 (2025).
- [36] Y. Chen, X. Liu, H.-Z. Lu, and X. C. Xie, Electrical switching of altermagnetism, *Phys. Rev. Lett.* **135**, 016701 (2025).
- [37] X. Duan, J. Zhang, Z. Zhu, Y. Liu, Z. Zhang, I. Žutić, and T. Zhou, Antiferroelectric altermagnets: Antiferroelectricity alters magnets, *Phys. Rev. Lett.* **134**, 106801 (2025).
- [38] J. Sodequist and T. Olsen, Two-dimensional altermagnets from high throughput computational screening: Symmetry requirements, chiral magnons, and spin-orbit effects, *Appl. Phys. Lett.* **124** (2024).
- [39] Z.-F. Gao, S. Qu, B. Zeng, Y. Liu, J.-R. Wen, H. Sun, P.-J. Guo, and Z.-Y. Lu, Ai-accelerated discovery of altermagnetic materials, *Natl. Sci. Rev.* **12**, nwaf066 (2025).
- [40] R. Bhattarai, P. Minch, and T. D. Rhone, High-throughput screening of altermagnetic materials, *Phys. Rev. Mater.* **9**, 064403 (2025).
- [41] A. B. Hellenes, T. Jungwirth, R. Jaeschke-Ubiergo, A. Chakraborty, J. Sinova, and L. Šmejkal, P-wave magnets, *arXiv:2309.01607* (2023).
- [42] Q. Song, S. Stavrić, P. Barone, A. Droghetti, D. S. Antonenko, J. W. Venderbos, C. A. Occhialini, B. Ilyas, E. Ergeçen, N. Gedik, *et al.*, Electrical switching of a p -wave magnet, *Nature*, **1** (2025).
- [43] Y. Yu, M. B. Lyngby, T. Shishidou, M. Roig, A. Kreisel, M. Weinert, B. M. Andersen, and D. F. Agterberg, Odd-parity magnetism driven by antiferromagnetic exchange, *Phys. Rev. Lett.* **135**, 046701 (2025).
- [44] B. Brekke, P. Sukhachov, H. G. Giil, A. Brataas, and J. Linder, Minimal models and transport properties of unconventional p -wave magnets, *Phys. Rev. Lett.* **133**, 236703 (2024).
- [45] M. Ezawa, Third-order and fifth-order nonlinear spin-current generation in g -wave and i -wave altermagnets and perfectly nonreciprocal spin current in f -wave magnets, *Phys. Rev. B* **111**, 125420 (2025).
- [46] Y.-P. Lin, Odd-parity altermagnetism through sublattice currents: From haldane-hubbard model to general bipartite lattices, *arXiv:2503.09602* (2025).
- [47] I. Žutić, J. Fabian, and S. Das Sarma, Spintronics: Fundamentals and applications, *Rev. Mod. Phys.* **76**, 323 (2004).
- [48] X. Zhang, Q. Liu, J.-W. Luo, A. J. Freeman, and A. Zunger, Hidden spin polarization in inversion-symmetric bulk crystals, *Nat. Phys.* **10**, 387 (2014).
- [49] A. Manchon, H. C. Koo, J. Nitta, S. M. Frolov, and R. A. Duine, New perspectives for rashba spin-orbit coupling, *Nat. Phys.* **14**, 871 (2015).
- [50] H. C. Koo, S. B. Kim, H. Kim, T.-E. Park, J. W. Choi, K.-W. Kim, G. Go, J. H. Oh, D.-K. Lee, E.-S. Park, *et al.*, Rashba effect in functional spintronic devices, *Adv. Mater.* **32**, 2002117 (2020).
- [51] A. J. Leggett, A theoretical description of the new phases of liquid ^3He , *Rev. Mod. Phys.* **47**, 331 (1975).
- [52] C. C. Tsuei and J. R. Kirtley, Pairing symmetry in cuprate superconductors, *Rev. Mod. Phys.* **72**, 969 (2000).
- [53] A. P. Mackenzie and Y. Maeno, The superconductivity of Sr_2RuO_4 and the physics of spin-triplet pairing, *Rev. Mod. Phys.* **75**, 657 (2003).
- [54] C.-K. Chan, Y.-T. Oh, J. H. Han, and P. A. Lee, Type-II weyl cone transitions in driven semimetals, *Phys. Rev. B* **94**, 121106 (2016).
- [55] Z. Yan and Z. Wang, Tunable weyl points in periodically driven nodal line semimetals, *Phys. Rev. Lett.* **117**, 087402 (2016).
- [56] K. Saha, Photoinduced chern insulating states in semi-dirac materials, *Phys. Rev. B* **94**, 081103 (2016).
- [57] A. Eckardt, Colloquium: Atomic quantum gases in periodically driven optical lattices, *Rev. Mod. Phys.* **89**, 011004 (2017).
- [58] H. Hübener, M. A. Sentef, U. De Giovannini, A. F. Kemper, and A. Rubio, Creating stable floquet-weyl semimetals by laser-driving of 3d dirac materials, *Nat. Commun.* **8**, 13940 (2017).
- [59] H. Liu, J.-T. Sun, C. Cheng, F. Liu, and S. Meng, Photoinduced nonequilibrium topological states in strained black phosphorus, *Phys. Rev. Lett.* **120**, 237403 (2018).
- [60] H. Liu, J.-T. Sun, and S. Meng, Engineering dirac states in graphene: Coexisting type-I and type-II floquet-dirac fermions, *Phys. Rev. B* **99**, 075121 (2019).
- [61] X.-S. Li, C. Wang, M.-X. Deng, H.-J. Duan, P.-H. Fu, R.-Q. Wang, L. Sheng, and D. Y. Xing, Photon-induced weyl half-metal phase and spin filter effect from topological dirac semimetals, *Phys. Rev. Lett.* **123**, 206601 (2019).
- [62] T. Oka and S. Kitamura, Floquet engineering of quantum materials, *Annu. Rev. Condens. Matter Phys.* **10**, 387 (2019).
- [63] M. S. Rudner and N. H. Lindner, Band structure engineering and non-equilibrium dynamics in floquet topological insulators,

- Nat. Rev. Phys. **2**, 229 (2020).
- [64] C. Bao, P. Tang, D. Sun, and S. Zhou, Light-induced emergent phenomena in 2d materials and topological materials, *Nat. Rev. Phys.* **4**, 33 (2022).
- [65] F. Zhan, R. Chen, Z. Ning, D.-S. Ma, Z. Wang, D.-H. Xu, and R. Wang, Perspective: Floquet engineering topological states from effective models towards realistic materials, *Quantum Frontiers* **3**, 21 (2024).
- [66] S. Huang, F. Zhan, X. Ding, D.-H. Xu, D.-S. Ma, and R. Wang, Controllable weyl nodes and fermi arcs from floquet engineering triple fermions, *Phys. Rev. B* **110**, L121118 (2024).
- [67] T. V. Trevisan, P. V. Arribi, O. Heinonen, R.-J. Slager, and P. P. Orth, Bicircular light floquet engineering of magnetic symmetry and topology and its application to the dirac semimetal Cd_3As_2 , *Phys. Rev. Lett.* **128**, 066602 (2022).
- [68] Z. Ning, D.-S. Ma, J. Zeng, D.-H. Xu, and R. Wang, Flexible control of chiral superconductivity in optically driven nodal point superconductors with antiferromagnetism, *Phys. Rev. Lett.* **133**, 246606 (2024).
- [69] See the Supplemental Material for the details of DFT computation, detailed discussion on spin degeneracy in CPL irradiated conventional antiferromagnets with $[\mathcal{C}_2 \parallel \mathcal{O}, \mathcal{O} \in \{\tau, \mathcal{M}_z\}]$, lattice model of *Category-II* and *Category-III*, *p*-wave spin splitting in FeCl_2 , list of material candidates of realizing light-induced odd-parity magnetism, which includes Refs. [71–93].
- [70] B. Li, D.-F. Shao, and A. A. Kovalev, Floquet spin splitting and spin generation in antiferromagnets, *arXiv* (2025), 2507.22884.
- [71] P. Hohenberg and W. Kohn, Inhomogeneous electron gas, *Phys. Rev.* **136**, B864 (1964).
- [72] W. Kohn and L. J. Sham, Self-consistent equations including exchange and correlation effects, *Phys. Rev.* **140**, A1133 (1965).
- [73] P. E. Blöchl, Projector augmented-wave method, *Phys. Rev. B* **50**, 17953 (1994).
- [74] J. P. Perdew, K. Burke, and M. Ernzerhof, Generalized gradient approximation made simple, *Phys. Rev. Lett.* **77**, 3865 (1996).
- [75] A. A. Mostofi, J. R. Yates, Y.-S. Lee, I. Souza, D. Vanderbilt, and N. Marzari, wannier90: A tool for obtaining maximally-localised wannier functions, *Comput. Phys. Commun.* **178**, 685 (2008).
- [76] Q. Wu, S. Zhang, H.-F. Song, M. Troyer, and A. A. Soluyanov, WannierTools: An open-source software package for novel topological materials, *Comput. Phys. Commun.* **224**, 405 (2018).
- [77] G. Long, H. Henck, M. Gibertini, D. Dumcenco, Z. Wang, T. Taniguchi, K. Watanabe, E. Giannini, and A. F. Morpurgo, Persistence of magnetism in atomically thin MnPS_3 crystals, *Nano Lett.* **20**, 2452 (2020).
- [78] N. Sivadas, M. W. Daniels, R. H. Swendsen, S. Okamoto, and D. Xiao, Magnetic ground state of semiconducting transition-metal trichalcogenide monolayers, *Phys. Rev. B* **91**, 235425 (2015).
- [79] Z. D. Vatansever, Y. Z. Abdullahi, F. Ersan, and E. Vatansever, Electronic, magnetic and universality properties of room-temperature antiferromagnet Fe_2O_3 monolayer, *J. Phys. Chem. Solids* **192**, 112080 (2024).
- [80] D.-S. Ko, W.-J. Lee, S. Sul, C. Jung, D.-J. Yun, H.-G. Kim, W.-J. Son, J. G. Chung, D. W. Jung, S. Y. Kim, *et al.*, Understanding the structural, electrical, and optical properties of monolayer *h*-phase RuO_2 nanosheets: a combined experimental and computational study, *NPG Asia Mater.* **10**, 266 (2018).
- [81] S. Sattar, M. F. Islam, and C. M. Canali, Monolayer MnX and janus XMnY ($X, Y = \text{S, Se, Te}$): A family of two-dimensional antiferromagnetic semiconductors, *Phys. Rev. B* **106**, 085410 (2022).
- [82] N. Fathizadeh, M. Modarresi, M. R. Roknabadi, J. Pawłowski, and A. Mogulkoc, Room-temperature antiferromagnetic order in monolayer Fe_2C , *Phys. Rev. B* **106**, 174423 (2022).
- [83] X. Yang, N. Ding, J. Chen, Z. Wang, M. An, and S. Dong, Electrical tuning of robust layered antiferromagnetism in MXene monolayer, *Appl. Phys. Lett.* **122**, 162403 (2023).
- [84] W. Zhou, G. Zheng, A. Li, D. Zhang, and F. Ouyang, Orbital contribution to the regulation of the spin-valley coupling in antiferromagnetic monolayer MnPTe_3 , *Phys. Rev. B* **107**, 035139 (2023).
- [85] M. Aapro, M. N. Huda, J. Karthikeyan, S. Kezilebieke, S. C. Ganguli, H. G. Herrero, X. Huang, P. Liljeroth, and H.-P. Komsa, Synthesis and properties of monolayer MnSe with unusual atomic structure and antiferromagnetic ordering, *ACS nano* **15**, 13794 (2021).
- [86] N. Guo, X. Fan, Z. Chen, Z. Luo, Y. Hu, Y. An, D. Yang, and S. Ma, Electronic and magnetic properties of group-V tmds monolayers with defects: a first-principles study, *Comput. Mater. Sci* **176**, 109540 (2020).
- [87] Y. Deng, Y. Yu, M. Z. Shi, Z. Guo, Z. Xu, J. Wang, X. H. Chen, and Y. Zhang, Quantum anomalous hall effect in intrinsic magnetic topological insulator MnBi_2Te_4 , *Science* **367**, 895 (2020).
- [88] J. Li, Y. Li, S. Du, Z. Wang, B.-L. Gu, S.-C. Zhang, K. He, W. Duan, and Y. Xu, Intrinsic magnetic topological insulators in van der waals layered MnBi_2Te_4 -family materials, *Sci. Adv* **5**, eaaw5685 (2019).
- [89] M. Lan, G. Xiang, Y. Nie, D. Yang, and X. Zhang, The static and dynamic magnetic properties of monolayer iron dioxide and iron dichalcogenides, *RSC Adv.* **6**, 31758 (2016).
- [90] J. Zhang, Y. Dai, and T. Zhang, Ferroelectric metals in van der waals bilayers, *Appl. Phys. Lett.* **124** (2024).
- [91] B. Zhou, Z. Li, J. Wang, and K. Wang, Superior spin-polarized electronic structure in $\text{MoS}_2/\text{MnO}_2$ heterostructures with an efficient hole injection, *Phys. Chem. Chem. Phys.* **21**, 10706 (2019).
- [92] P. Zhou, C. Sun, and L. Sun, Two dimensional antiferromagnetic chern insulator: NiRuCl_6 , *Nano Lett.* **16**, 6325 (2016).
- [93] J. Li, C. Xie, W. Wang, X.-P. Li, G. Zhang, and X. Wang, Antiferromagnetic second-order topology in two-dimensional NiRuCl_6 , *Appl. Phys. Lett.* **123** (2023).

Supplemental materials of “Light-induced Odd-parity Magnetism in Conventional Collinear Antiferromagnets”

This supplementary material is organized in five sections. In the first section, we provide the details of DFT calculations in the main text. In the second section, we clarify the spin degeneracy in light-irradiated conventional AFM with $[\mathcal{C}_2 \parallel \mathcal{O}', \mathcal{O}' \in \{\tau, \mathcal{M}_z\}]$. In the third section, we give more in-depth discussion on light-irradiated hexagonal lattices with tight-binding models. In the fourth section, we show the intrinsic band structures of materials in the main text. In the fifth section, we show the p -wave spin splitting in FeCl_2 induced by BCL, EPL, and strain. The last section provides the list of material candidates for achieving odd-parity spin splitting.

DFT CALCULATIONS

We employed density functional theory (DFT) [71, 72] within the Vienna Ab initio Simulation Package (VASP) using the projector augmented-wave method [73]. The generalized gradient approximation (GGA) [74] of Perdew-Burke-Ernzerhof type was used to account for the exchange-correction potential. The kinetic-energy cutoff was set to 500 eV, and a $18 \times 18 \times 1$ Γ -centered k -point mesh was used for all calculations. A criterion of energy different in electronic self-consistent calculation is set to 10^{-8} eV. The lattice constants are fully relaxed and converged below 10^{-3} eV/Å for residual force.

To utilize Floquet laser light field in our material system, we first projected the plane waves basis for first-principle calculations to maximally localized Wannier functions (MLWF) basis, with the help of Wannier90 [75, 76].

The Wannier tight-binding Hamiltonian we gain can be expressed as

$$H(\mathbf{r}) = \sum_{mn} \sum_j t_j^{mn} C_m^\dagger(\mathbf{R}_j) C_n(\mathbf{R}_0) + h.c. \quad (8)$$

where t_j^{mn} is the hopping amplitude from m localized Wannier orbital of site R_0 to n localized Wannier orbital of site R_j . The operator $C_m^\dagger(R_j)$ ($C_m(R_0)$) create and (annihilates) a electron on respected sites. The vector potential $\mathbf{A}(t) = \mathbf{A}(t + T)$ of time-periodic CPL coupled to the Hamiltonian by Peierls substitution as.

$$t_j^{mn}(t) = t_j^{mn} e^{i \frac{e}{\hbar} \mathbf{A}(t) \cdot \mathbf{d}_{mn}} \quad (9)$$

Where \mathbf{d}_{mn} is the relative position vector between two Wannier orbitals. Thus we obtained the time-dependent Hamiltonian as

$$H(k, t) = \sum_{mn} \sum_j t_j^{mn}(t) e^{ik \cdot \mathbf{R}_j} C_m^\dagger(k, t) C_n(k, t) + h.c. \quad (10)$$

Due to the translation symmetry of both the time and lattice, Floquet theorem can be effectively applied to the time-dependent Hamiltonian. Thus we express the Floquet-Bloch creation (annihilation) operator as

$$C_m^\dagger(k, t) = \sum_j \sum_{\alpha=-\infty}^{\infty} C_{\alpha m}^\dagger(\mathbf{R}_j) e^{+ik \cdot \mathbf{R}_j - i\alpha\omega t} \quad (11)$$

$$C_m(k, t) = \sum_j \sum_{\alpha=-\infty}^{\infty} C_{\alpha m}(\mathbf{R}_j) e^{-ik \cdot \mathbf{R}_j + i\alpha\omega t} \quad (12)$$

Thus, we gain an effective static Hamiltonian in frequency and momentum space

$$H(k, \omega) = \sum_{m,n} \sum_{\alpha,\beta} [H_{\alpha-\beta}^{mn} + H_\Omega] C_{\alpha m}^\dagger(k) C_{\beta n}(k) + h.c. \quad (13)$$

with

$$H_{\alpha-\beta}^{mn} = \sum_j e^{ik \cdot \mathbf{R}_j} \frac{1}{T} \int_0^T t_j^{mn} e^{i \frac{e}{\hbar} \mathbf{A}(t) \cdot \mathbf{d}_{mn}} e^{i(\alpha-\beta)\omega t} dt \quad (14)$$

$$H_\Omega = \alpha \hbar \omega \delta_{mn} \delta_{\alpha\beta} \quad (15)$$

where $\hbar\omega$ represent the photon energy, (α, β) is the Floquet index ranging from $-\infty$ to ∞ . Then the effective Floquet-Bloch Hamiltonian can be described as

$$H_{\text{eff}}(\mathbf{k}, \omega) = H_0(\mathbf{k}, \omega) + \frac{[H_1(\mathbf{k}, \omega), H_{-1}(\mathbf{k}, \omega)]}{\omega} + \mathcal{O}\left(\frac{1}{\omega^2}\right). \quad (16)$$

SPIN DEGENERACY IN LIGHT-IRRADIATED CONVENTIONAL AFM WITH $[C_2 \parallel \mathcal{O}', \mathcal{O}' \in \{\tau, \mathcal{M}_z\}]$

In this section, we demonstrate that circularly polarized light cannot induce spin splitting in antiferromagnetic systems with $[C_2 \parallel \mathcal{O}', \mathcal{O}' \in \{\tau, \mathcal{M}_z\}]$ symmetry. We begin with a tight-binding model on an AFM hexagonal lattice belonging to space group $P\bar{6}$ (No. 174), as illustrated in Fig. 4. Magnetic atoms occupy the Wyckoff position $2h$ at $(1/3, 2/3, z)$, while additional nonmagnetic atoms reside at the $2i$ position: $(2/3, 1/3, z)$. The spin degeneracy in such conventional antiferromagnets is protected by the spin-space group symmetry $[C_2 \parallel \mathcal{M}_z]$. Two key points are noteworthy: (i) the mirror symmetry \mathcal{M}_z maps (x, y, z) to $(x, y, -z)$; (ii) the z -component of the time-periodic gauge field $\mathbf{A}(t)$ vanishes. As a result, the two magnetic sublattices with opposite magnetic moment respond identically under light irradiation, thereby precluding spin splitting. Figs. 4(b)-(c) demonstrate that, even $H'(\mathbf{k})$ is non-zero, the energy bands of $H_{\text{AFM}}(\mathbf{k})$, $H_0(\mathbf{k})$, and $H_{\text{eff}}(\mathbf{k})$ exhibit band-degenerate characteristics. Similarly, in case of antiferromagnetic systems with $[C_2 \parallel \tau]$ symmetry, there is no light-induced spin splitting.

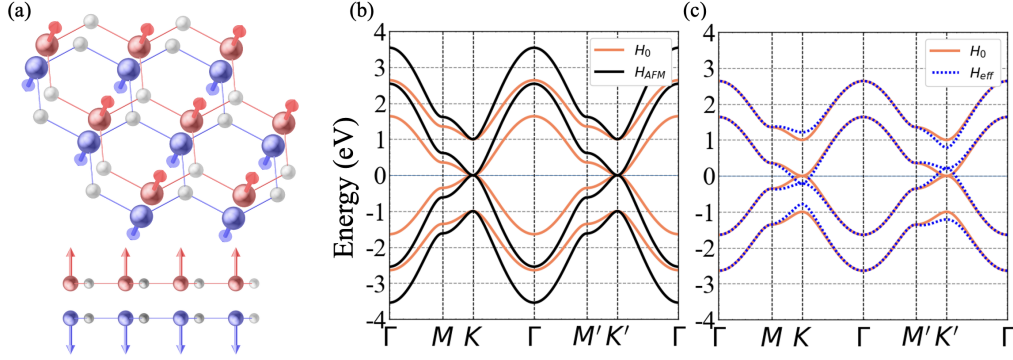


FIG. 4. CPL-irradiated conventional AFM with $[C_2 \parallel \mathcal{O}', \mathcal{O}' \in \{\tau, \mathcal{M}_z\}]$. (a) The illustration figure of AFM bilayer honeycomb lattice with $[C_2 \parallel \mathcal{M}_z]$. (b)-(c) The spin-degenerate energy spectra of $H_{\text{AFM}}(\mathbf{k})$ and $H_0(\mathbf{k})$ and $H_{\text{eff}}(\mathbf{k})$. The parameters of nearest neighbor hopping $t = 1$ eV and magnetic moment $m = 1$ eV and the light intensity of $eA_0/\hbar = 0.5 \text{ \AA}^{-1}$ are adopted.

SPIN DEGENERACY AND SPIN SPLITTING IN LIGHT IRRADIATED HEXAGONAL LATTICES

In this section, we give more detailed discussion on the honeycomb lattice tight-binding model in the third section of the main text. The model in the main text is

$$H = t \sum_{\langle i,j \rangle} c_i^\dagger c_j + \sum_i c_i^\dagger [\mu_\zeta \sigma_0 + \mathbf{m}_\zeta \cdot \boldsymbol{\sigma}] c_i + h.c., \quad (17)$$

which can be expressed in momentum space as, under the basis $[\varphi_\uparrow^A, \varphi_\uparrow^B, \varphi_\downarrow^A, \varphi_\downarrow^B]$,

$$H_{\text{AFM}}(\mathbf{k}) = \begin{bmatrix} 0 & \Delta(\mathbf{k}) \\ \Delta(\mathbf{k})^* & 0 \end{bmatrix} \tau_0 + (|m_\zeta| \sigma_z + |\mu_\zeta| \sigma_0) \tau_z \quad (18)$$

with $\Delta(\mathbf{k}) = t \sum_i e^{i\mathbf{k} \cdot \boldsymbol{\delta}_i}$, and $\boldsymbol{\delta}_i (i = 1, 2, 3)$ are the nearest-neighbor vectors.

linear polarized light irradiated AFM honeycomb lattice

First, we show that spin-splitting can not be induced by linear polarized light (LPL). We apply an LPL irradiated along the z direction with x -axis polarization to AFM honeycomb lattice model Eq. (18). With straightforward derivation, combining Eq. (14) and Eq. (16), one has $H_1(\mathbf{k}, \omega) = -H_{-1}(\mathbf{k}, \omega)$, which results in $[H_1(\mathbf{k}), H_{-1}(\mathbf{k})] = \omega H'(\mathbf{k}) = 0$. Thus, as shown in Fig. 5, with the light intensity of $eA_0/\hbar = 0.5 \text{ \AA}^{-1}$ as an example, the band structure of the LPL irradiated AFM honeycomb lattice is spin-degenerate.

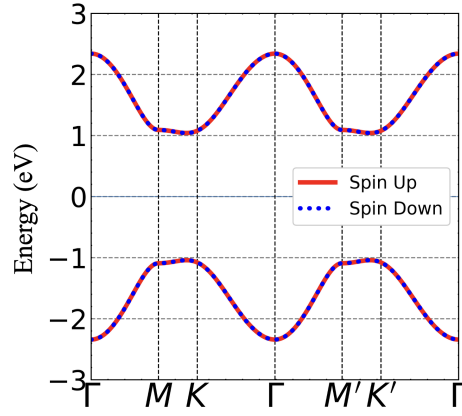


FIG. 5. The band structure of the lattice model in Eq.2 of the main text under LPL with a vector potential $\mathbf{A}_{\text{LPL}}(t) = (A_x \sin \omega t, 0, 0)$. The parameters $t = m_\zeta = 1$ eV, $\mu_\zeta = 0$, and the light intensity of $eA_0/\hbar = 0.5 \text{ \AA}^{-1}$ are adopted.

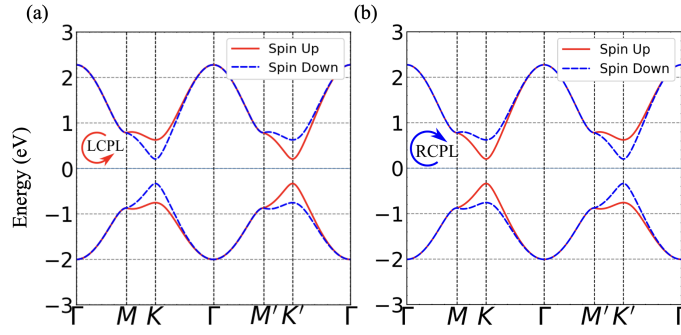


FIG. 6. The CPL irradiated band structure for the lattice model in Eq. (19) of the main text with additional next nearest-neighbor hopping t_{NN} . The parameters $t = 1$ eV, $t_2 = 0.1$ eV, $m_1 = -m_2 = 0.5$ eV, $\mu_\zeta = 0$, and the light intensity of $eA_0/\hbar = 0.5 \text{ \AA}^{-1}$ are adopted.

CPL irradiated AFM honeycomb lattice with next nearest couplings

Next, we add the additional next nearest hopping term t_2 to the Hamilton as

$$H = t \sum_{\langle i,j \rangle} c_i^\dagger c_j + t_2 \sum_{\langle\langle i,j \rangle\rangle} c_i^\dagger c_j + \sum_i c_i^\dagger [\mu_\zeta \sigma_0 + \mathbf{m}_\zeta \cdot \boldsymbol{\sigma}] c_i + h.c., \quad (19)$$

where $\langle\langle i,j \rangle\rangle$ is the next nearest neighbor, the Hamiltonian in momentum space can be written in the same form as

$$H_{\text{AFM2}}(\mathbf{k}) = \begin{bmatrix} \Delta_2(\mathbf{k}) & \Delta(\mathbf{k}) \\ \Delta(\mathbf{k})^* & \Delta_2(\mathbf{k}) \end{bmatrix} \tau_0 + (|m_\zeta| \sigma_z + |\mu_\zeta| \sigma_0) \tau_z \quad (20)$$

with $\Delta_2(\mathbf{k}) = t_2 \sum_j e^{i\mathbf{k} \cdot \boldsymbol{\delta}'_j}$, and $\boldsymbol{\delta}'_j (j = 1, 2, 3, 4, 5, 6)$ are the six next nearest-neighbor vectors. In Fig. 6, we show that the spin-resolved band structure of left- and right-handed CPL irradiated hexangular AFM lattice with the next nearest-neighbor couplings are taken into account. The spin-degenerate system is found to exhibit f -wave spin splitting under light irradiation. In Figs. 6(a)-(b) confirm that changing the chirality of CPL can reverse the spin polarization order.

Odd-parity spin splitting realized in light irradiated van der Waals magnetic multilayer

Next, we turn to the case of AFM multilayers, by stacking the AFM model in Eq. (18) and add inter-layer hopping t_i . Under the basis $[\varphi_{\uparrow}^{A1}, \varphi_{\uparrow}^{B1}, \dots, \varphi_{\uparrow}^{An}, \varphi_{\uparrow}^{Bn}, \varphi_{\downarrow}^{A1}, \varphi_{\downarrow}^{B1}, \dots, \varphi_{\downarrow}^{An}, \varphi_{\downarrow}^{Bn}]$, we write the Hamiltonian in momentum space as

$$H_{\text{AFM}}^n(\mathbf{k}) = \tau_0 I_n \begin{bmatrix} 0 & \Delta(\mathbf{k}) \\ \Delta(\mathbf{k})^* & 0 \end{bmatrix} + \tau_z I_n (|m_\zeta| \sigma_z + |\mu_\zeta| \sigma_0) + t_i \tau_0 M_n \sigma_0, \quad (21)$$

where I_n denotes the identity matrix of order n , M_n is $n \times n$ matrix with elements read as $M_{ij} = \begin{cases} 1 & |i-j| = 1 \\ 0 & |i-j| \neq 1 \end{cases}$, and n is the number of layers. In Fig. 7, we show that the CPL induce spin splitting in van der Waals magnetic bilayer and triple-layer systems.

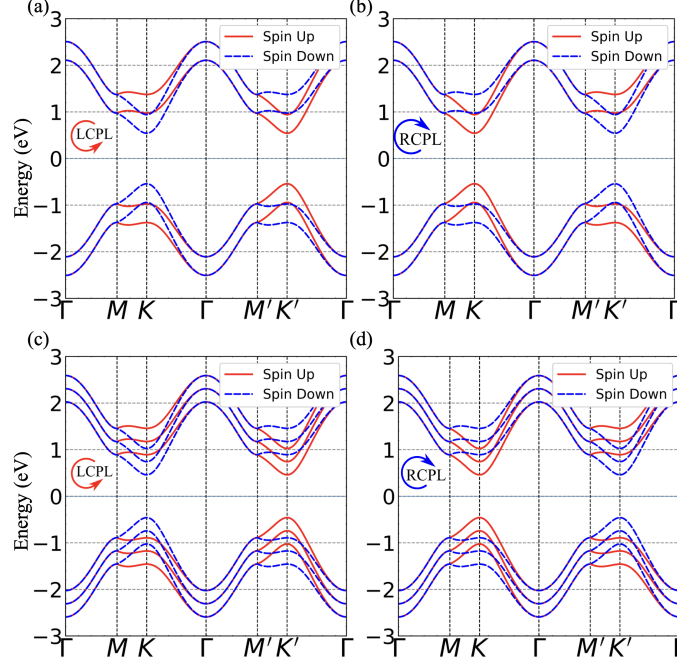


FIG. 7. Odd-parity spin splitting realized in light irradiated van der Waals magnetic multilayer. (a)-(b) The band structure of bilayer case in Eq. (18) under right and left-handed CPL. (c)-(d) The band structure of tri-layers case in Eq. (18) under right and left-handed CPL the parameters $t = 1$ eV, $t_i = 0.2$ eV, $m_1 = -m_2 = 1$ eV, $\mu_\zeta = 0$, and the light intensity of $eA_0/\hbar = 0.5 \text{ \AA}^{-1}$ are adopted.

Model Hamiltonian of Category-II and Category-III

Next we turn to the AFM bilayers composed of magnetic monolayers which is referred as *Category-II* and *Category-III* in the main text. Under the basis $[\varphi_{\uparrow}^{A1}, \varphi_{\uparrow}^{B1}, \varphi_{\uparrow}^{A2}, \varphi_{\uparrow}^{B2}, \varphi_{\downarrow}^{A1}, \varphi_{\downarrow}^{B1}, \varphi_{\downarrow}^{A2}, \varphi_{\downarrow}^{B2}]$, we write the Hamiltonian in momentum space as

$$H_{\text{AFM}}^n(\mathbf{k}) = \tau_0 I_2 \begin{bmatrix} 0 & \Delta(\mathbf{k}) \\ \Delta(\mathbf{k})^* & 0 \end{bmatrix} + \tau_z (iM' |m_\zeta| \sigma_z + I_2 |\mu_\zeta| \sigma_0) + t_i \tau_0 M_2 \sigma_0, \quad (22)$$

where M' is the second Pauli matrix indicates the interlayer AFM order. When $m_1 \neq 0$ & $m_2 = 0$ ($m_1 \neq m_2 \neq 0$), the van der Waals magnetic bilayer system is classified as *Category-II* (*Category-III*) in the main text. The CPL induced f -wave spin splitting in these two kinds of lattice model are shown in Fig. 8. Notably, when $m_1 = m_2 = 0$ the two sublattice can be connected by $[C_2 || \mathcal{M}_z]$, indicating the absence of spin splitting as shown in Figs. 8 (e)-(f).

THE SPIN DEGENERACY IN INTRINSIC AFM MnPS₃, FeCl₂, AND NiRuCl₆

Fig. 9 demonstrates that the energy bands of these three materials are intrinsically spin-degenerate in the absence of a light field and spin-orbital coupling.

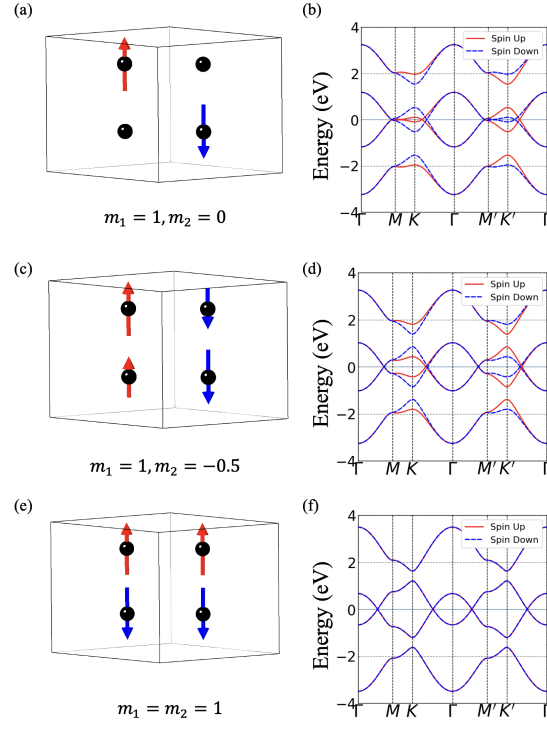


FIG. 8. The spin-splitting and degeneracy in AFM bilayers. (a)-(b) The magnetic configuration and CPL irradiated band structure of *Category-II* AFM bilayers. (c)-(d) The magnetic configuration and CPL irradiated band structure of *Category-III* AFM bilayers. (e)-(f) The magnetic configuration and CPL irradiated band structure AFM bilayers with $[C_2 \parallel \mathcal{M}_z]$ symmetry. The parameters $t = 1$ eV, $t_i = 0.1$ eV, $\mu_\zeta = 0$, and the light intensity of $eA_0/\hbar = 0.5 \text{ \AA}^{-1}$ are adopted.

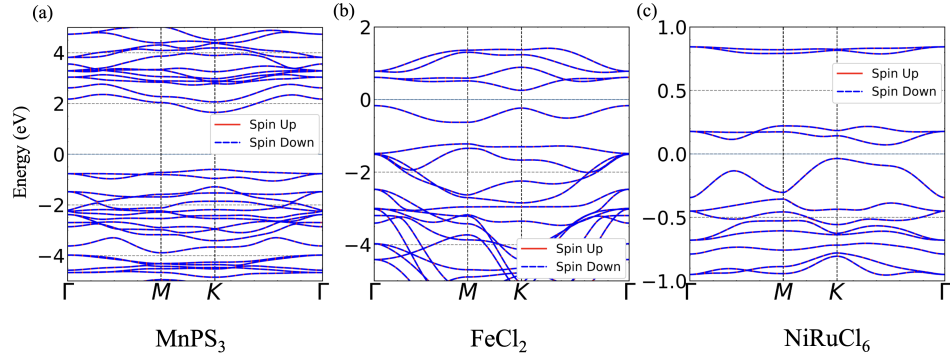


FIG. 9. The intrinsic spin-degenerate band structure of (a) MnPS₃ monolayer, (b) AFM FeCl₂ bilayer, and (c) AFM NiRuCl₆ bilayer without spin-orbital coupling.

THE p -WAVE SPIN SPLITTING IN FeCl₂ INDUCED BY BCL, EPL, AND STRAIN

In Figs. 10-11, we take the AFM FeCl₂ bilayer as an example to show that the BCL, EPL, and strain combined with CPL can induce p -wave spin splitting.

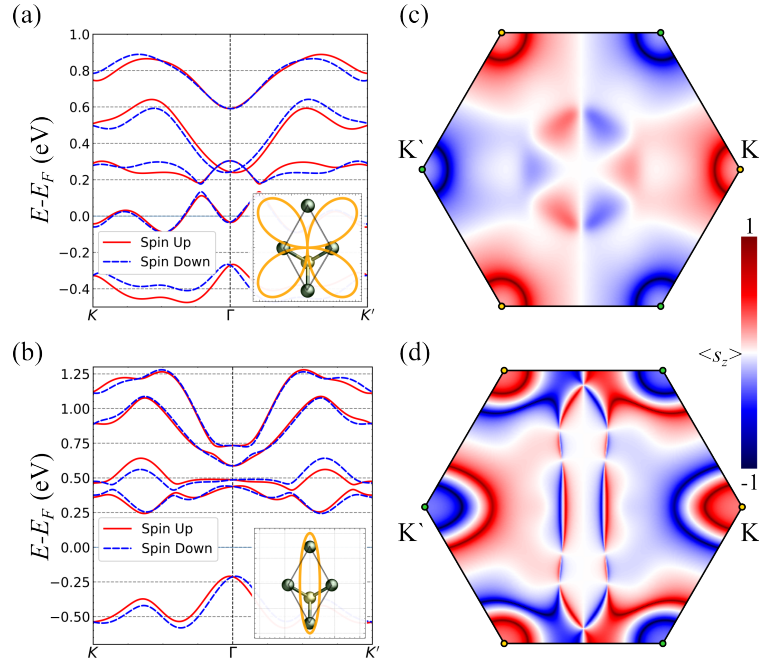


FIG. 10. BCPL and EPL induced p -wave spin-splitting for FeCl_2 bilayer. (a)-(b) The band along high-symmetry lines of the FeCl_2 bilayer under BCPL and EPL with a light intensity of $eA_0/\hbar = 0.3 \text{ \AA}^{-1}$. The insert in each figure shown the relative orientation of light polarization pattern and FeCl_2 lattice. (c)-(d) The spin-resolved p -wave isoenergy surface at 0.5 eV of FeCl_2 bilayer corresponding to (a) and (b)

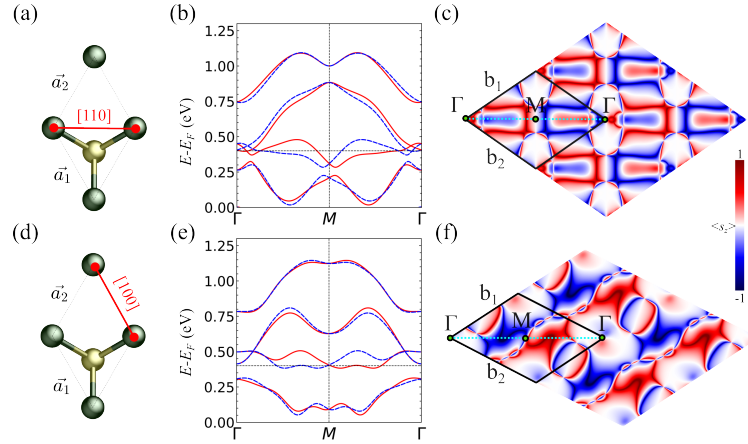


FIG. 11. CPL induced p -wave spin-splitting for strain applied FeCl_2 bilayer. (a)-(c) CPL irradiated FeCl_2 bilayer with 20% tensile strain along $[110]$ direction. (d)-(f) CPL irradiated FeCl_2 bilayer with 20% tensile strain along $[100]$ direction. (a) and (d) are the illustration figure of corresponding strain. In (b) and (e) the spin-resolved band structures are shown for both cases. (c) and (f) are The spin-resolved p -wave isoenergy surface at 0.4 eV for both cases. A CPL with the light intensity of $eA_0/\hbar = 0.3 \text{ \AA}^{-1}$ are adopted.

MATERIAL CANDIDATES

In this section, we list some material candidates for light-induced f -wave spin-splitting. All of the materials listed in Table I have been experimentally or computationally reported to have magnetic order that required to realize odd-parity spin splitting.

TABLE I. The material candidates for Floquet induced odd-parity spin-splitting

Type	Material	Space group (for monolayer of <i>Category</i> -II and III)
<i>Category</i> -I	MnPS ₃ , MnPSe ₃ [77, 78]	$P\bar{3}1m$
<i>Category</i> -I	Fe ₂ O ₃ [79]	$P\bar{3}1m$
<i>Category</i> -I	MnX (X = S, Se, Te)[81]	$P\bar{3}m1$
<i>Category</i> -I	Fe ₂ C[82]	$P\bar{3}1m$
<i>Category</i> -I	Cr ₂ CCl ₂ [83]	$P\bar{3}m1$
<i>Category</i> -I	MnPTe ₃ [84]	$P\bar{3}1m$
<i>Category</i> -I	BL-MnBi ₂ Te ₄ [87, 88]	$P\bar{3}m1$
<i>Category</i> -II	1H-RuO ₂ [80]	$P\bar{6}m2$
<i>Category</i> -II	1H-MX ₂ (M = V, Nb, Ta; X = S, Se, Te)[86]	$P\bar{6}m2$
<i>Category</i> -II	1H-FeX ₂ (X = O, S, Se, Te)[89]	$P\bar{6}m2$
<i>Category</i> -II	1H-MnX ₂ (X = O, Te)[90, 91]	$P\bar{6}m2$
<i>Category</i> -III	NiRuCl ₆ [92, 93]	$P321$

* donghuixu@cqu.edu.cn

† mads@cqu.edu.cn

‡ rewang@cqu.edu.cn

- [1] S. Hayami, Y. Yanagi, and H. Kusunose, Bottom-up design of spin-split and reshaped electronic band structures in antiferromagnets without spin-orbit coupling: Procedure on the basis of augmented multipoles, *Phys. Rev. B* **102**, 144441 (2020).
- [2] H. Bai, L. Han, X. Y. Feng, Y. J. Zhou, R. X. Su, Q. Wang, L. Y. Liao, W. X. Zhu, X. Z. Chen, F. Pan, X. L. Fan, and C. Song, Observation of spin splitting torque in a collinear antiferromagnet RuO₂, *Phys. Rev. Lett.* **128**, 197202 (2022).
- [3] I. Mazin (The PRX Editors), Editorial: Altermagnetism—a new punch line of fundamental magnetism, *Phys. Rev. X* **12**, 040002 (2022).
- [4] C. Wu, K. Sun, E. Fradkin, and S.-C. Zhang, Fermi liquid instabilities in the spin channel, *Phys. Rev. B* **75**, 115103 (2007).
- [5] R. D. Gonzalez Betancourt, J. Zubáć, R. Gonzalez-Hernandez, K. Geishendorf, Z. Šobáň, G. Springholz, K. Olejník, L. Šmejkal, J. Sinova, T. Jungwirth, S. T. B. Goennenwein, A. Thomas, H. Reichlová, J. Železný, and D. Kriegner, Spontaneous anomalous hall effect arising from an unconventional compensated magnetic phase in a semiconductor, *Phys. Rev. Lett.* **130**, 036702 (2023).
- [6] S. Hayami, Y. Yanagi, and H. Kusunose, Momentum-dependent spin splitting by collinear antiferromagnetic ordering, *J. Phys. Soc. Jpn* **88**, 123702 (2019).
- [7] P. A. McClarty and J. G. Rau, Landau theory of altermagnetism, *Phys. Rev. Lett.* **132**, 176702 (2024).
- [8] J. Krempaský, L. Šmejkal, S. D'souza, M. Hajlaoui, G. Springholz, K. Uhlířová, F. Alarab, P. Constantinou, V. Strocov, D. Usanov, *et al.*, Altermagnetic lifting of kramers spin degeneracy, *Nature* **626**, 517 (2024).
- [9] L. Bai, W. Feng, S. Liu, L. Šmejkal, Y. Mokrousov, and Y. Yao, Altermagnetism: Exploring new frontiers in magnetism and spintronics, *Adv. Funct. Mater* **34**, 2409327 (2024).
- [10] C. Song, H. Bai, Z. Zhou, L. Han, H. Reichlova, J. H. Dil, J. Liu, X. Chen, and F. Pan, Altermagnets as a new class of functional materials, *Nat. Rev. Mater.* , 1 (2025).
- [11] S.-W. Cheong and F.-T. Huang, Altermagnetism classification, *npj Quantum Mater.* **10**, 38 (2025).
- [12] F. Zhang, X. Cheng, Z. Yin, C. Liu, L. Deng, Y. Qiao, Z. Shi, S. Zhang, J. Lin, Z. Liu, *et al.*, Crystal-symmetry-paired spin–valley locking in a layered room-temperature metallic altermagnet candidate, *Nat. Phys.* , 1 (2025).
- [13] M. Hu, X. Cheng, Z. Huang, and J. Liu, Catalog of *c*-paired spin-momentum locking in antiferromagnetic systems, *Phys. Rev. X* **15**, 021083 (2025).
- [14] W. Brinkman and R. J. Elliott, Theory of spin-space groups, *Proc. R. Soc. A* **294**, 343 (1966).
- [15] P. Liu, J. Li, J. Han, X. Wan, and Q. Liu, Spin-group symmetry in magnetic materials with negligible spin-orbit coupling, *Phys. Rev. X* **12**, 021016 (2022).
- [16] L. Šmejkal, J. Sinova, and T. Jungwirth, Emerging research landscape of altermagnetism, *Phys. Rev. X* **12**, 040501 (2022).
- [17] Z. Xiao, J. Zhao, Y. Li, R. Shindou, and Z.-D. Song, Spin space groups: Full classification and applications, *Phys. Rev. X* **14**, 031037 (2024).
- [18] Y. Jiang, Z. Song, T. Zhu, Z. Fang, H. Weng, Z.-X. Liu, J. Yang, and C. Fang, Enumeration of spin-space groups: Toward a complete description of symmetries of magnetic orders, *Phys. Rev. X* **14**, 031039 (2024).
- [19] L. Šmejkal, R. González-Hernández, T. Jungwirth, and J. Sinova, Crystal time-reversal symmetry breaking and spontaneous hall effect in collinear antiferromagnets, *Sci. Adv.* **6**, eaaz8809 (2020).
- [20] L. Šmejkal, J. Sinova, and T. Jungwirth, Beyond conventional ferromagnetism and antiferromagnetism: A phase with nonrelativistic spin and crystal rotation symmetry, *Phys. Rev. X* **12**, 031042 (2022).
- [21] L. Šmejkal, A. B. Hellenes, R. González-Hernández, J. Sinova, and T. Jungwirth, Giant and tunneling magnetoresistance in unconventional collinear antiferromagnets with nonrelativistic spin-momentum coupling, *Phys. Rev. X* **12**, 011028 (2022).
- [22] D.-F. Shao, S.-H. Zhang, M. Li, C.-B. Eom, and E. Y. Tsymlal, Spin-neutral currents for spintronics, *Nat. Commun.* **12**, 7061 (2021).
- [23] X. Zhou, W. Feng, X. Yang, G.-Y. Guo, and Y. Yao, Crystal chirality magneto-optical effects in collinear antiferromagnets, *Phys. Rev. B* **104**, 024401 (2021).

- [24] H.-Y. Ma, M. Hu, N. Li, J. Liu, W. Yao, J.-F. Jia, and J. Liu, Multifunctional antiferromagnetic materials with giant piezomagnetism and noncollinear spin current, *Nat. Commun.* **12**, 2846 (2021).
- [25] T. Aoyama and K. Ohgushi, Piezomagnetic properties in altermagnetic mnte, *Phys. Rev. Mater.* **8**, L041402 (2024).
- [26] H. Reichlova, R. Lopes Seeger, R. González-Hernández, I. Kounta, R. Schlitz, D. Kriegner, P. Ritzinger, M. Lammel, M. Leiviskä, A. Birk Hellenes, *et al.*, Observation of a spontaneous anomalous hall response in the Mn_3Si_3 d-wave altermagnet candidate, *Nat. Commun.* **15**, 4961 (2024).
- [27] R. He, D. Wang, N. Luo, J. Zeng, K.-Q. Chen, and L.-M. Tang, Nonrelativistic spin-momentum coupling in antiferromagnetic twisted bilayers, *Phys. Rev. Lett.* **130**, 046401 (2023).
- [28] B. Pan, P. Zhou, P. Lyu, H. Xiao, X. Yang, and L. Sun, General stacking theory for altermagnetism in bilayer systems, *Phys. Rev. Lett.* **133**, 166701 (2024).
- [29] Y. Liu, J. Yu, and C.-C. Liu, Twisted magnetic van der waals bilayers: An ideal platform for altermagnetism, *Phys. Rev. Lett.* **133**, 206702 (2024).
- [30] S. Zeng and Y.-J. Zhao, Bilayer stacking a -type altermagnet: A general approach to generating two-dimensional altermagnetism, *Phys. Rev. B* **110**, 174410 (2024).
- [31] X. Zhu, X. Huo, S. Feng, S.-B. Zhang, S. A. Yang, and H. Guo, Design of altermagnetic models from spin clusters, *Phys. Rev. Lett.* **134**, 166701 (2025).
- [32] C. W. J. Beenakker and T. Vakhel, Phase-shifted andreev levels in an altermagnet josephson junction, *Phys. Rev. B* **108**, 075425 (2023).
- [33] J. A. Ouassou, A. Brataas, and J. Linder, dc josephson effect in altermagnets, *Phys. Rev. Lett.* **131**, 076003 (2023).
- [34] D. Zhu, Z.-Y. Zhuang, Z. Wu, and Z. Yan, Topological superconductivity in two-dimensional altermagnetic metals, *Phys. Rev. B* **108**, 184505 (2023).
- [35] M. Gu, Y. Liu, H. Zhu, K. Yananose, X. Chen, Y. Hu, A. Stroppa, and Q. Liu, Ferroelectric switchable altermagnetism, *Phys. Rev. Lett.* **134**, 106802 (2025).
- [36] Y. Chen, X. Liu, H.-Z. Lu, and X. C. Xie, Electrical switching of altermagnetism, *Phys. Rev. Lett.* **135**, 016701 (2025).
- [37] X. Duan, J. Zhang, Z. Zhu, Y. Liu, Z. Zhang, I. Žutić, and T. Zhou, Antiferroelectric altermagnets: Antiferroelectricity alters magnets, *Phys. Rev. Lett.* **134**, 106801 (2025).
- [38] J. Sodequist and T. Olsen, Two-dimensional altermagnets from high throughput computational screening: Symmetry requirements, chiral magnons, and spin-orbit effects, *Appl. Phys. Lett.* **124** (2024).
- [39] Z.-F. Gao, S. Qu, B. Zeng, Y. Liu, J.-R. Wen, H. Sun, P.-J. Guo, and Z.-Y. Lu, Ai-accelerated discovery of altermagnetic materials, *Nat. Sci. Rev.* **12**, nwaf066 (2025).
- [40] R. Bhattacharai, P. Minch, and T. D. Rhone, High-throughput screening of altermagnetic materials, *Phys. Rev. Mater.* **9**, 064403 (2025).
- [41] A. B. Hellenes, T. Jungwirth, R. Jaeschke-Ubiergo, A. Chakraborty, J. Sinova, and L. Šmejkal, P-wave magnets, *arXiv:2309.01607* (2023).
- [42] Q. Song, S. Stavrić, P. Barone, A. Droghetti, D. S. Antonenko, J. W. Venderbos, C. A. Occhialini, B. Ilyas, E. Ergeçen, N. Gedik, *et al.*, Electrical switching of a p -wave magnet, *Nature*, **1** (2025).
- [43] Y. Yu, M. B. Lyngby, T. Shishidou, M. Roig, A. Kreisel, M. Weinert, B. M. Andersen, and D. F. Agterberg, Odd-parity magnetism driven by antiferromagnetic exchange, *Phys. Rev. Lett.* **135**, 046701 (2025).
- [44] B. Brekke, P. Sukhachov, H. G. Giil, A. Brataas, and J. Linder, Minimal models and transport properties of unconventional p -wave magnets, *Phys. Rev. Lett.* **133**, 236703 (2024).
- [45] M. Ezawa, Third-order and fifth-order nonlinear spin-current generation in g -wave and i -wave altermagnets and perfectly nonreciprocal spin current in f -wave magnets, *Phys. Rev. B* **111**, 125420 (2025).
- [46] Y.-P. Lin, Odd-parity altermagnetism through sublattice currents: From haldane-hubbard model to general bipartite lattices, *arXiv:2503.09602* (2025).
- [47] I. Žutić, J. Fabian, and S. Das Sarma, Spintronics: Fundamentals and applications, *Rev. Mod. Phys.* **76**, 323 (2004).
- [48] X. Zhang, Q. Liu, J.-W. Luo, A. J. Freeman, and A. Zunger, Hidden spin polarization in inversion-symmetric bulk crystals, *Nat. Phys.* **10**, 387 (2014).
- [49] A. Manchon, H. C. Koo, J. Nitta, S. M. Frolov, and R. A. Duine, New perspectives for rashba spin-orbit coupling, *Nat. Phys.* **14**, 871 (2015).
- [50] H. C. Koo, S. B. Kim, H. Kim, T.-E. Park, J. W. Choi, K.-W. Kim, G. Go, J. H. Oh, D.-K. Lee, E.-S. Park, *et al.*, Rashba effect in functional spintronic devices, *Adv. Mater.* **32**, 2002117 (2020).
- [51] A. J. Leggett, A theoretical description of the new phases of liquid ^3He , *Rev. Mod. Phys.* **47**, 331 (1975).
- [52] C. C. Tsuei and J. R. Kirtley, Pairing symmetry in cuprate superconductors, *Rev. Mod. Phys.* **72**, 969 (2000).
- [53] A. P. Mackenzie and Y. Maeno, The superconductivity of Sr_2RuO_4 and the physics of spin-triplet pairing, *Rev. Mod. Phys.* **75**, 657 (2003).
- [54] C.-K. Chan, Y.-T. Oh, J. H. Han, and P. A. Lee, Type-II weyl cone transitions in driven semimetals, *Phys. Rev. B* **94**, 121106 (2016).
- [55] Z. Yan and Z. Wang, Tunable weyl points in periodically driven nodal line semimetals, *Phys. Rev. Lett.* **117**, 087402 (2016).
- [56] K. Saha, Photoinduced chern insulating states in semi-dirac materials, *Phys. Rev. B* **94**, 081103 (2016).
- [57] A. Eckardt, Colloquium: Atomic quantum gases in periodically driven optical lattices, *Rev. Mod. Phys.* **89**, 011004 (2017).
- [58] H. Hübener, M. A. Sentef, U. De Giovannini, A. F. Kemper, and A. Rubio, Creating stable floquet-weyl semimetals by laser-driving of 3d dirac materials, *Nat. Commun.* **8**, 13940 (2017).
- [59] H. Liu, J.-T. Sun, C. Cheng, F. Liu, and S. Meng, Photoinduced nonequilibrium topological states in strained black phosphorus, *Phys. Rev. Lett.* **120**, 237403 (2018).
- [60] H. Liu, J.-T. Sun, and S. Meng, Engineering dirac states in graphene: Coexisting type-I and type-II floquet-dirac fermions, *Phys. Rev. B* **99**, 075121 (2019).
- [61] X.-S. Li, C. Wang, M.-X. Deng, H.-J. Duan, P.-H. Fu, R.-Q. Wang, L. Sheng, and D. Y. Xing, Photon-induced weyl half-metal phase and spin filter effect from topological dirac semimetals, *Phys. Rev. Lett.* **123**, 206601 (2019).
- [62] T. Oka and S. Kitamura, Floquet engineering of quantum materials, *Annu. Rev. Condens. Matter Phys.* **10**, 387 (2019).

- [63] M. S. Rudner and N. H. Lindner, Band structure engineering and non-equilibrium dynamics in floquet topological insulators, *Nat. Rev. Phys.* **2**, 229 (2020).
- [64] C. Bao, P. Tang, D. Sun, and S. Zhou, Light-induced emergent phenomena in 2d materials and topological materials, *Nat. Rev. Phys.* **4**, 33 (2022).
- [65] F. Zhan, R. Chen, Z. Ning, D.-S. Ma, Z. Wang, D.-H. Xu, and R. Wang, Perspective: Floquet engineering topological states from effective models towards realistic materials, *Quantum Frontiers* **3**, 21 (2024).
- [66] S. Huang, F. Zhan, X. Ding, D.-H. Xu, D.-S. Ma, and R. Wang, Controllable weyl nodes and fermi arcs from floquet engineering triple fermions, *Phys. Rev. B* **110**, L121118 (2024).
- [67] T. V. Trevisan, P. V. Arribi, O. Heinonen, R.-J. Slager, and P. P. Orth, Bicircular light floquet engineering of magnetic symmetry and topology and its application to the dirac semimetal Cd_3As_2 , *Phys. Rev. Lett.* **128**, 066602 (2022).
- [68] Z. Ning, D.-S. Ma, J. Zeng, D.-H. Xu, and R. Wang, Flexible control of chiral superconductivity in optically driven nodal point superconductors with antiferromagnetism, *Phys. Rev. Lett.* **133**, 246606 (2024).
- [69] See the Supplemental Material for the details of DFT computation, detailed discussion on spin degeneracy in CPL irradiated conventional antiferromagnets with $[\mathcal{C}_2 || \mathcal{O}, \mathcal{O} \in \{\tau, \mathcal{M}_z\}]$, lattice model of *Category-II* and *Category-III*, *p*-wave spin splitting in FeCl_2 , list of material candidates of realizing light-induced odd-parity magnetism, which includes Refs. [71–93].
- [70] B. Li, D.-F. Shao, and A. A. Kovalev, Floquet spin splitting and spin generation in antiferromagnets, *arXiv* (2025), 2507.22884.
- [71] P. Hohenberg and W. Kohn, Inhomogeneous electron gas, *Phys. Rev.* **136**, B864 (1964).
- [72] W. Kohn and L. J. Sham, Self-consistent equations including exchange and correlation effects, *Phys. Rev.* **140**, A1133 (1965).
- [73] P. E. Blöchl, Projector augmented-wave method, *Phys. Rev. B* **50**, 17953 (1994).
- [74] J. P. Perdew, K. Burke, and M. Ernzerhof, Generalized gradient approximation made simple, *Phys. Rev. Lett.* **77**, 3865 (1996).
- [75] A. A. Mostofi, J. R. Yates, Y.-S. Lee, I. Souza, D. Vanderbilt, and N. Marzari, wannier90: A tool for obtaining maximally-localised wannier functions, *Comput. Phys. Commun.* **178**, 685 (2008).
- [76] Q. Wu, S. Zhang, H.-F. Song, M. Troyer, and A. A. Soluyanov, WannierTools: An open-source software package for novel topological materials, *Comput. Phys. Commun.* **224**, 405 (2018).
- [77] G. Long, H. Henck, M. Gibertini, D. Duncenco, Z. Wang, T. Taniguchi, K. Watanabe, E. Giannini, and A. F. Morpurgo, Persistence of magnetism in atomically thin MnPS_3 crystals, *Nano Lett.* **20**, 2452 (2020).
- [78] N. Sivadas, M. W. Daniels, R. H. Swendsen, S. Okamoto, and D. Xiao, Magnetic ground state of semiconducting transition-metal trichalcogenide monolayers, *Phys. Rev. B* **91**, 235425 (2015).
- [79] Z. D. Vatansever, Y. Z. Abdullahi, F. Ersan, and E. Vatansever, Electronic, magnetic and universality properties of room-temperature antiferromagnet Fe_2O_3 monolayer, *J. Phys. Chem. Solids* **192**, 112080 (2024).
- [80] D.-S. Ko, W.-J. Lee, S. Sul, C. Jung, D.-J. Yun, H.-G. Kim, W.-J. Son, J. G. Chung, D. W. Jung, S. Y. Kim, *et al.*, Understanding the structural, electrical, and optical properties of monolayer *h*-phase RuO_2 nanosheets: a combined experimental and computational study, *NPG Asia Mater.* **10**, 266 (2018).
- [81] S. Sattar, M. F. Islam, and C. M. Canali, Monolayer MnX and janus XMnY ($X, Y = \text{S, Se, Te}$): A family of two-dimensional antiferromagnetic semiconductors, *Phys. Rev. B* **106**, 085410 (2022).
- [82] N. Fathizadeh, M. Modarresi, M. R. Roknabadi, J. Pawłowski, and A. Mogulkoc, Room-temperature antiferromagnetic order in monolayer Fe_2C , *Phys. Rev. B* **106**, 174423 (2022).
- [83] X. Yang, N. Ding, J. Chen, Z. Wang, M. An, and S. Dong, Electrical tuning of robust layered antiferromagnetism in MXene monolayer, *Appl. Phys. Lett.* **122**, 162403 (2023).
- [84] W. Zhou, G. Zheng, A. Li, D. Zhang, and F. Ouyang, Orbital contribution to the regulation of the spin-valley coupling in antiferromagnetic monolayer MnPTe_3 , *Phys. Rev. B* **107**, 035139 (2023).
- [85] M. Aapro, M. N. Huda, J. Karthikeyan, S. Kezilebieke, S. C. Ganguli, H. G. Herrero, X. Huang, P. Liljeroth, and H.-P. Komsa, Synthesis and properties of monolayer MnSe with unusual atomic structure and antiferromagnetic ordering, *ACS nano* **15**, 13794 (2021).
- [86] N. Guo, X. Fan, Z. Chen, Z. Luo, Y. Hu, Y. An, D. Yang, and S. Ma, Electronic and magnetic properties of group-V tmds monolayers with defects: a first-principles study, *Comput. Mater. Sci* **176**, 109540 (2020).
- [87] Y. Deng, Y. Yu, M. Z. Shi, Z. Guo, Z. Xu, J. Wang, X. H. Chen, and Y. Zhang, Quantum anomalous hall effect in intrinsic magnetic topological insulator MnBi_2Te_4 , *Science* **367**, 895 (2020).
- [88] J. Li, Y. Li, S. Du, Z. Wang, B.-L. Gu, S.-C. Zhang, K. He, W. Duan, and Y. Xu, Intrinsic magnetic topological insulators in van der waals layered MnBi_2Te_4 -family materials, *Sci. Adv* **5**, eaaw5685 (2019).
- [89] M. Lan, G. Xiang, Y. Nie, D. Yang, and X. Zhang, The static and dynamic magnetic properties of monolayer iron dioxide and iron dichalcogenides, *RSC Adv.* **6**, 31758 (2016).
- [90] J. Zhang, Y. Dai, and T. Zhang, Ferroelectric metals in van der waals bilayers, *Appl. Phys. Lett.* **124** (2024).
- [91] B. Zhou, Z. Li, J. Wang, and K. Wang, Superior spin-polarized electronic structure in $\text{MoS}_2/\text{MnO}_2$ heterostructures with an efficient hole injection, *Phys. Chem. Chem. Phys.* **21**, 10706 (2019).
- [92] P. Zhou, C. Sun, and L. Sun, Two dimensional antiferromagnetic chern insulator: NiRuCl_6 , *Nano Lett.* **16**, 6325 (2016).
- [93] J. Li, C. Xie, W. Wang, X.-P. Li, G. Zhang, and X. Wang, Antiferromagnetic second-order topology in two-dimensional NiRuCl_6 , *Appl. Phys. Lett.* **123** (2023).